Discovery of specific HDAC6 inhibitor with anti-metastatic effects in pancreatic cancer cells through virtual screening and biological evaluation

Haoxuan Song[a], Xueyan Niu[a], Jishun Quan[b], Yanchun Li[a], Lei Yuan[b], Jian Wang[b], Chao Ma[b,*], Enlong Ma[a,*]

[a] School of Life Sciences and Biopharmaceutical Science, Shenyang Pharmaceutical University, 103 Wenhua Road, Shenhe District, Shenyang 110016, PR China
[b] Key Laboratory of Structure-Based Drug Design & Discovery of Ministry of Education, School of Pharmaceutical Engineering, Shenyang Pharmaceutical University, 103 Wenhua Road, Shenhe District, Shenyang 110016, PR China

ARTICLE INFO

ABSTRACT

Histone deacetylase 6 (HDAC6) has been demonstrated to play a major role in cell motility and aggresome formation, and HDAC6 inhibition is therefore considered as a promising epigenetic strategy for cancer treatment. At present, only a minority of compounds have been reported as HDAC6 inhibitors, so specific HDAC6 inhibitors with safety profile need to be discovered urgently. In this paper, HDAC6 inhibitors with diverse structures were used to generate the pharmacophore model by ligand-based method, which contained two hydrogen bond acceptors and two hydrophobic groups. A combined virtual screening based on pharmacophore model and molecular docking was adopted to screen potential HDAC6 inhibitors. Subsequently, the HDAC6 inhibitory activity of the hit compounds were evaluated using an *in vitro* enzyme binding inhibition assay. The experimental results illustrated that cefoperazone sodium had the strongest inhibitory effect on HDAC6 among the six screened compounds, and its IC_{50} value was 8.59 ± 1.06 μM. Cefoperazone sodium significantly catalyzed the hyperacetylation of α-tubulin but not histone H3, proving that cefoperazone sodium was a selective inhibitor of HDAC6. Since the expression of HDAC6 plays an important role in cancer metastasis, the effects of cefoperazone sodium on migration and invasion of human pancreatic cancer PANC-1 cells were further investigated by wound healing and transwell chamber assays. It was found that cefoperazone sodium could evidently inhibit the migration and invasion of PANC-1 cells. Furthermore, the binding pattern of inhibitor at the active site of the crystal structure was revealed by molecular docking, providing a reference value for the structural design and optimization of HDAC6 inhibitors. This study provides a systematic virtual screening approach for discovering HDAC6 active inhibitors, and by which the specific effect of cefoperazone sodium against HDAC6 was found, suggesting its potential application on cancer therapy.

1. Introduction

Histone deacetylase (HDAC) plays a significant role in the structural modification of chromosomes and the regulation of gene expression. The acetylation of histones facilitates the dissociation of DNA and histone octamer. It also makes the relaxation of nucleosome structure, thereby various transcription factors and synergistic transcription factors are able to specifically bind to DNA sites and ultimately activate the transcription of genes. Under normal circumstances, histone acetylation and histone deacetylation in the nucleus are in dynamic equilibrium, which are regulated by histone deacetylases and histone acetyltransferases [1]. However, under pathological conditions, HDACs are in an overexpressed state. Several recent studies have shown that histone

deacetylase inhibition is a promising epigenetic strategy for cancer treatment. Currently, FDA approved HDAC inhibitors including vorinostat, romidepsin, panobinostat, chidamide and belinostat. However, most broad-spectrum HDAC inhibitors [2], including the clinically approved agents, have side effects such as nausea, vomiting, and myelosuppression [3,4]. Accordingly, the development of HDAC inhibitors have shifted from early broad-spectrum HDAC inhibitors to selective HDAC inhibitors.

Human HDAC isozymes can be divided into four categories depending on structure: class I HDACs (1–3, 8); class IIa HDACs (4, 5, 7, 9) and class IIb HDACs (6, 10); class III HDACs, better known as sirtuins; and the sole class IV enzyme, HDAC11. Class I, II and IV are Zn^{2+} dependent proteases, while class III is NAD^+ dependent [5]. HDAC6 is

the only HDACs member with two functional catalytic domains (CD1 and CD2), and CD2 domain is more critical for lysine deacetylase activity of HDAC6. HDAC6 is able to specifically catalyze non-histone substrates, including cortactin, α-tubulin and heat shock protein 90 (Hsp90) [6], and it can participate in tumorigenesis, development and metastasis through various pathways such as tubulin [7], Hsp90 and protein ubiquitination. Selective HDAC6 inhibitors have little cytotoxicity to normal cells, which are expected to overcome the shortcomings of broad-spectrum HDAC inhibitors. Only a few compounds have been reported as specific HDAC6 inhibitors so far, for instance, ACY-1215 [8], Tubastatin A [9], Tubacin [10] and Nexturastat A [11]. Due to various adverse reactions of broad-spectrum HDAC inhibitors and the scarcity of HDAC6 inhibitors, specific HDAC6 inhibitors with safety profile need to be discovered urgently.

Computer-aided drug design has been recognized as an effective method for the discovery of targeted drugs [12], and the pharmacophore approach has become one of the main tools for drug discovery and can be used for drug design and virtual screening. Ligand-based virtual screening can utilize a common pharmacophore model to reveal the structural requirements for biological activities. The procedure for the discovery of HDAC6 active compounds in this study is shown in Fig. 1. We first established the pharmacophore model of HDAC6 inhibitors by summarizing the key characteristics of ligands with diverse structures, and the reliability of pharmacophore model was validated through decoy set subsequently. Virtual screening combined with pharmacophore model was used to identify selective HDAC6 inhibitors from FDA Drugs Database. The screened compounds were docked with the crystal structure of HDAC6 via molecular docking to exclude the false positive and improve the hit rate in the databases screening. We performed a preliminary screening for the HDAC6 inhibitory activities of the 6 hit compounds in molecular docking, and found that cefoperazone sodium had the strongest inhibitory effect on HDAC6. Afterwards, immunoblotting analysis showed that cefoperazone sodium could selectively inhibit HDAC6 in the cellular environment. Therefore, cefoperazone sodium was regarded as a specific HDAC6 inhibitor. Further experiments demonstrated its inhibitory effect on tumor metastasis *in vitro*. In general, this work provides a systematic approach to identify HDAC6 active inhibitors, which has important clinical significance for the development of new HDAC6 inhibitors for cancer treatment.
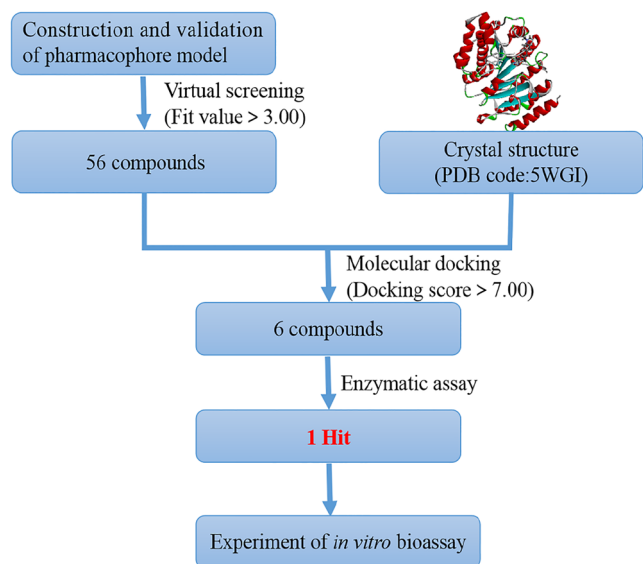

Fig. 1. The schematic diagram of active compound discovery based on virtual screening and biological assays.

2. Materials and methods

2.1. Common feature-based 3D pharmacophore modelling

All calculations were conducted on a Dell Power Edge R910 server under the RHEL5 platform. Discovery Studio 3.0 (DS 3.0) software package (BIOVIA Inc) was used to generate pharmacophore and Glide 9.7 extra precision (XP) with Schrödinger package [13] was applied for docking studies.

2.1.1. Construction of common feature pharmacophore

The pharmacophore model in this study was obtained from 34 molecule compounds [8,9,11,14–22] with diverse scaffolds and activity values, which IC_{50} values ranged from 0.26 nM to 1 mM. The training set, including 16 HDAC6 inhibitors selected according to the diversity of molecular structures, was used to establish the common-feature pharmacophore models. The remaining 18 HDAC6 inhibitors were used as a decoy set to validate pharmacophore models.

Ligand structures were prepared and consistency tests were performed on all atoms and bond types. The reported active compounds were optimized by LigPrep protocol of Maestro software before the generation of pharmacophore hypothesis. Optimization includes the addition of hydrogen atoms, the adjustment of the compounds to the appropriate protonation state at pH 5 to 9 and the steepest descent method to optimize the molecular geometric conformation at the OPLS_2005 force field [23]. In this research, the characteristic mapping includes five chemical features, i.e., hydrophobic group (H), hydrogen bond donor (D), aromatic ring (R), hydrogen bond acceptor (A) and positive ionizable center (P). During the formation of the simulated pharmacophores, the maximum features value was set to 10 and the minimum value was set to 1. Based on the activity of training set molecules, the "Principal" value was set to 2 or 0 (The active compounds were set to 2, while the inactive compounds were set to 0), and the "MaxOmitFeat" value was set to 1. Other parameters were set as default parameters. Afterwards, 10 pharmacophore hypotheses were built utilizing the Common Feature Pharmacophore Generation tool implemented in DS 3.0.

2.1.2. Validation of the pharmacophore model

The pharmacophore models were further validated through decoy set by fit values, including 14 active HDAC6 inhibitors and 4 inactive inhibitors. Ligand Profiler module was employed to map the decoy set to pharmacophores, and the fit values were matched with the heat map to verify the accuracy of the pharmacophore models. According to these data, an optimal pharmacophore model can be selected to distinguish active inhibitors from inactive ones.

2.2. Virtual screening and molecular docking

2.2.1. Database screening based on built pharmacophore model

An optimal pharmacophore model was used in a 3D structural query to screen the selective HDAC6 inhibitors from FDA Drugs Database. The Ligand Pharmacophore Mapping protocol was applied to virtual screening, and its parameter settings were the same as the decoy set verification. The index 'fit value' was scaled to a range of 0.0–4.0 to rank the screened compounds. Adding the weight value of each feature in the pharmacophore to get the maximum fit. The screened compounds with the 'fit value' > 3.0 were retained.

2.2.2. Molecular docking

Molecular docking is a significant simulation method for collecting the probable conformations of small molecule compounds involved in receptor interactions at its active site [24]. In addition, this method can also be used to predict the binding free energy and the possible binding modes of the docked compounds. In the database screening based on pharmacophore model, a correct molecular docking method can

examine whether a ligand has good binding at the active site of a receptor protein, thus eliminating false positives and improving the hit rate. This step can scan a great quantity of molecules and make it a reasonable number of hits [25].

Many experimental crystal structures of HDAC6-ligand complexes have been reported before 2020 in the Protein Data Bank (http://www.rcsb.org/pdb/) [26], but current drug discovery efforts mainly focus on blocking catalytic activity of the HDAC6 CD2 domain. Crystal structure analysis reveals that CD2 domain of human HDAC6 is very similar to that of zebrafish, sharing over 75% of amino acid sequences. Zebrafish HDAC6 CD2 is a valid surrogate of human HDAC6 CD2. Our preliminary study (Table S1) showed that there was a large root-mean-square deviation while using the crystal structure (PDB code: 5EDU) of human HDAC6 CD2 to perform docking studies. 5WGI is an ultrahigh resolution crystal structure of zebrafish HDAC6 CD2, and its root-mean-square deviation is less than 2, which can maintain the binding mode of the co-crystallized ligand inside its protein. Therefore, the crystal structure of zebrafish HDAC6 (PDB code: 5WGI. Resolution: 1.05 Å) was used for molecular docking. Protein Preparation Wizard in the Schrödinger suite [27] was applied to process the HDAC6-ligand co-crystallized structure (PDB code: 5WGI) to prepare protein. The crystal structure of 5WGI included two identical chains, and we chosed A-chain as the subject investigated for further calculations. Because there was no water molecules existing any co-ordination with the ligand, water molecules and other cofactors were deleted. Both acidic and alkaline amino acid residues were processed into a suitable ionizing state at pH 7.4. Then HDAC6-ligand complexes were accurately assessed for energy using a force field OPLS_2005 restrained minimization with convergence of heavy atoms to a root-mean-square deviation (RMSD) of 0.3 Å. Other processes of preparation included preparing the receptor pocket of the crystal structure. Ultimately, the crystal structure and the co-crystallized ligand were separated for subsequent simulation.

The compounds were docked with the crystal structures using Glide 9.7 extra precision (XP) with Schrödinger package. The prepared protein–ligand complex was the receptor structure excluding the co-crystallized ligand whose position determined the coordinate of active site (the position of crystal structure pocket is x = 14 Å, y = 12 Å, z = 14 Å). It can be used to analyze the docking postures by checking their relative total energy score and the RMSD value. By using the selected docking procedure and crystal structure, the screening of molecular docking was performed for those compounds screened from FDA Drugs Database. The score of molecular docking can reflect the binding ability between the ligand and the protein. The docking results were visualized and analyzed with Discovery Studio 2017 software.

2.3. Enzyme binding inhibition assay

HDAC6 was diluted to 100 ng/ml with the buffer solution. All the assay components were diluted in HDAC6 assay buffer (including 25 mM Tris/HCl, pH 8.0, 137 mM NaCl, 2.7 mM KCl, 1 mM $MgCl_2$ and 0.1 mg/ml BSA), and 100 μM Ac-Lys (Ac)-AMC was used as the substrate. The enzyme was mixed with or without 20 μl of different concentrations of the sample in a 96-well plate, and then 20 μl of fluorescent substrate was added. After incubating at 37 °C for 120 min, 50 μl of developer was added into each well and incubated for 15 min at 37 °C to allow the fluorescence signal to develop. Fluorescence intensity of each well was measured using an automatic microplate reader at excitation and emission wavelengths of 380 nm and 460 nm, respectively. The enzyme binding inhibition can be observed by comparing the fluorescence intensity.

2.4. Cell culture

Human pancreatic cancer PANC-1 cells were cultured in Dulbecco's modified Eagle's medium (DMEM) supplemented with 10% fetal bovine serum (FBS), 100 U/ml penicillin and 100 μg/ml streptomycin. Cell lines were grown at 37 °C in 100% humidity and 5% CO_2.

2.5. MTT assay

The cells in the 96-well plates were treated with different concentrations of cefoperazone sodium or Tubacin, and 0.1% DMSO was used as the control group. After 48 h of cell culture, 5.0 mg/ml MTT solution was added and incubated at 37℃ for 4 h. The purple formazan crystals were dissolved in 150 μl DMSO and read at 490 nm on a microplate reader. The ratio of the absorbance of treated cells to the control groups could reflect cell viability. Statistical Product and Service Solutions software was used to calculate the IC_{50} values.

2.6. Immunoblotting analysis

PANC-1 cells were treated with cefoperazone sodium, pan-HDAC inhibitor SAHA and HDAC6 specific inhibitor tubacin for 48 h. Cells were washed twice with cold PBS, and incubated for 10 min in cold lysis buffer containing a protease inhibitor. The cells were scraped from the culture surface into prechilled tubes, and incubated on ice for 30 min. Afterwards, the tubes were centrifuged for 15 min at 12,000 g and 4 °C. The clarified supernatant was transferred to a fresh prechilled tube and kept it on ice. The amount of protein in the lysate was measured using BCA Protein Assay Kit. Protein samples were electrophoresed on 12% SDS-PAGE, transferred onto PVDF membranes, and blocked with 5% fat-free milk in TBS-0.10% Tween 20 (TBST) for 1 h at room temperature. The membranes were then incubated with the primary antibodies in 5% fat-free milk overnight at 4 °C, followed by incubation with HRP-conjugated secondary antibodies for 1 h at room temperature. The results of antibodies binding were imaged using the ECL detection reagent.

2.7. Detection of HDAC6 activity in cells

The activity of HDAC6 in cells was detected using BioVision's HDAC6 Activity Assay Kit (Catalog # K466-100). 2×10^4 cells treated with or without drugs in 2 ml medium were seeded into 6-well plates for 48 h. After washing with cold PBS, cells (2×10^6) were homogenized in 100 μl of HDAC6 lysis buffer on ice and incubated on ice for 5 min. The cytosolic fraction was prepared by centrifuging the lysate at 16,000 g for 10 min at 4 °C. Then, clarified supernatant was transferred to a fresh prechilled tube and kept it on ice. The amount of protein in the lysate or purified enzyme was measured using BCA Protein Assay Kit. The lysate was diluted with HDAC6 assay buffer. 10 μl of protein was added to 40 μl of chilled HDAC6 assay buffer, and 50 μl of specific HDAC6 substrate was transferred to each well of a 96-well plate. After incubating at 37 °C for 30 min in the dark, 10 μl of developer was added to each well. The 96-well plate was incubated at 37 °C for 10 min to generate fluorescence. The fluorescence intensity was measured using an automatic microplate reader (excitation wavelength 380 nm, emission wavelength 490 nm).

2.8. Wound healing assay

Human pancreatic cancer PANC-1 cells were seeded onto 6-well plates for the wound-healing assay. When the cells achieved 100% confluence, a single scratch was made across the cell monolayer using a micropipette tip, and the cells were washed to remove debris. Cells were incubated in fresh medium with or without cefoperazone sodium or HDAC6 inhibitor (Tubacin) for 48 h. Cell migration images were photographed by an inverted phase-contrast microscope at 0 and 48 h, and Image J software was used to quantify the migration results.

2.9. Transwell chamber assay

24-well Matrigel invasion chambers (BD Biosciences) were used for

Table 1
Common feature pharmacophore result was generated by the HipHop.

Hypothesis	Features[a]	Rank[b]	Direct Hit[c]	Partial Hit[d]	Partial Hit
01	HHDA	99.310	1111111111101111	0000000000010000	4
02	HHDA	99.277	1111111111101111	0000000000010000	4
03	HHDA	99.140	1111111111101111	0000000000010000	4
04	HHDA	98.001	1111111111101111	0000000000010000	4
05	HHAA	97.204	1111111111101111	0000000000010000	4
06	HHDA	96.972	1111111111101111	0000000000010000	4
07	HHAA	96.940	1111111111101111	0000000000010000	4
08	HHAA	96.332	1111111111101111	0000000000010000	4
09	HHDA	96.126	1111111111101111	0000000000010000	4
10	HHAA	95.801	1111111111101111	0000000000010000	4

NOTE: [a] H: hydrophobic, D:hydrogen bond donor, A: hydrogen bond acceptor. [b] The score of the hypothesis. [c] Direct Hit indicates whether ("1") or not ("0") a compound mapped every feature in the hypothesis. [d] Partial Hit indicates whether ("1") or not ("0") a compound mapped all but one feature in the hypothesis.
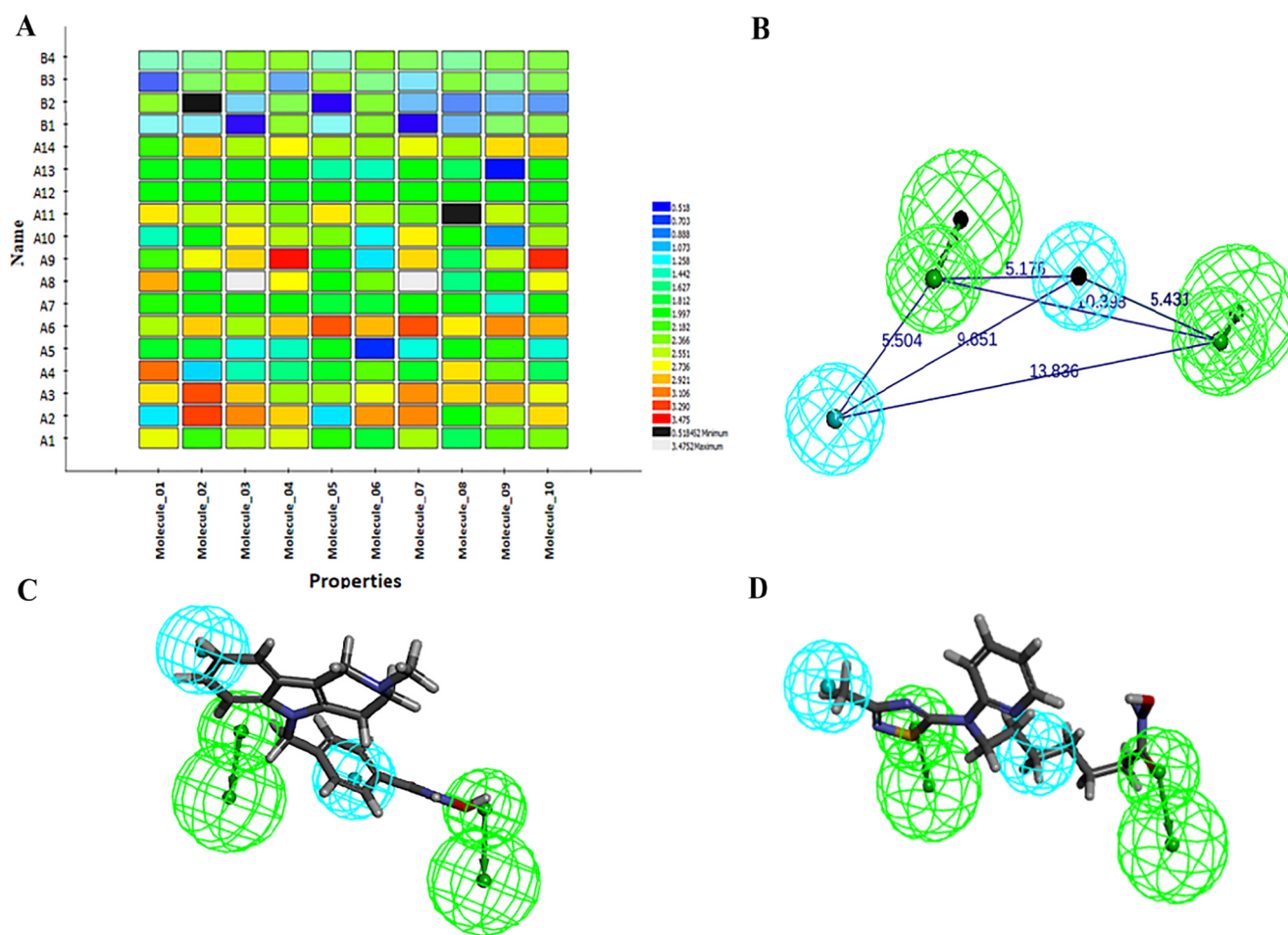

Fig. 2. The validation by heat map and its feature of the pharmacophore. (A) Heat map of Ligand profiler revealed hypothesis 7 as the best pharmacophore by the range of fit values. (B) The optimal pharmacophore model consists of two features: two hydrophobic groups H (blue) and two hydrogen bond acceptors A (green). Distances between the features are expressed in Å, with a tolerance of ± 0.8 Å. (C) The overlapping image between a known HDAC6 inhibitor (Tubastatin A) and pharmacophore model_07. (D) The overlapping image between the most active ligand A3 in the decoy set and pharmacophore model_07. (For interpretation of the references to colour in this figure legend, the reader is referred to the web version of this article.)

transwell chamber assays determination. After trypsinization, the cells were reseeded in the upper chamber at a concentration of 3×10^5 /ml in 200 µl of the medium with or without cefoperazone sodium or HDAC6 inhibitor (Tubacin). The medium supplemented with 10% FBS was added to the bottom well for 500 ml. Cells on the upper surface of the chamber were wiped off after 24 h of incubation, and on the lower surface were fixed with methanol and then stained with crystal violet.

3. Results and discussion

3.1. Construction and validation of pharmacophore model

In this article, a training set (Fig. S1) consisting of 16 molecules [28–30] with diverse scaffolds and wide range of HDAC6 inhibitory activity (Table S2) was used to generate the pharmacophore models. The HipHop process from the Catalyst software was used to compare

Table 2
Virtual screening results of pharmacophore model from the FDA Drugs Database.

No.	ZINC code	Fit value	No.	ZINC code	Fit value
1	03830301	3.68712	29	01587572	3.16726
2	03830417	3.58867	30	03830457	3.16505
3	03830398	3.52046	31	03830451	3.16223
4	03830760	3.51502	32	03830310	3.15896
5	03830430	3.48577	33	03830404	3.15788
6	03830672	3.45565	34	03830690	3.15008
7	03830460	3.43659	35	03830295	3.13212
8	03830671	3.42211	36	03830729	3.13131
9	01530775	3.38229	37	03830445	3.13127
10	03830495	3.34564	38	03830403	3.13096
11	03830673	3.33764	39	03830490	3.12917
12	03830432	3.32963	40	03830512	3.12239
13	03830395	3.32084	41	03830294	3.12114
14	03830759	3.29989	42	03830402	3.10836
15	01587572	3.28637	43	03830299	3.09382
16	03830302	3.28191	44	03830477	3.08954
17	03830484	3.26275	45	03830492	3.08466
18	03793076	3.24709	46	03830269	3.08334
19	03830429	3.24463	47	03830392	3.07856
20	03830847	3.23671	48	03830456	3.07068
21	03830260	3.23658	49	03830372	3.06489
22	00004319	3.23541	50	03830436	3.05749
23	03830508	3.23118	51	03830271	3.05369
24	03830731	3.21666	52	03830397	3.04437
25	01542915	3.19123	53	03830431	3.03419
26	03830373	3.18887	54	03830381	3.02894
27	03830420	3.18335	55	03830487	3.01768
28	03830504	3.18268	56	03830386	3.00795

Table 3
The hits from docking-based virtual screening.

No.	Docking score	ZINC code	CAS No.
1	−8.825	03830430	62893-20-3
2	−8.261	01530775	100-33-4
3	−7.914	03830847	31430-15-6
4	−7.736	03830484	56238-63-2
5	−7.578	01542915	52152-93-9
6	−7.255	00004319	32780-64-6

various inhibitors, and three-dimensional hypothesis based on common chemical characteristics were obtained. Afterwards, the common feature pharmacophore generation protocol HipHop algorithm of DS 3.0 was used to develop 10 pharmacophore hypotheses (Table 1) from the training set, and the 10 pharmacophores generated consist of four features. Two groups appeared based on hierarchical clustering of the 10 pharmacophore hypotheses: HHDA、HHAA.

In order to get a most accurate pharmacophore model, a decoy set (Fig. S2) which contained 14 active inhibitors of HDAC6 and 4 inactive inhibitors was used to validate the pharmacophore models. Through an intuitive visualization method, the heat map (Fig. 2A) can analyze the distribution of experimental data, and the fit values are represented by different colored bars. The orange and white blocks represent high fit values, and the green blocks represent medium fit values, while the black and blue blocks represent low fit values. According to the mapping results of pharmacophores, the hypothesis 7 (Fig. 2B) had significant distinction between active compounds and inactive compounds, which had better fit values with the active compounds (A1-A14) while poor fit values with the inactive compounds (B1-B4). The results indicated that the pharmacophore hypothesis 7, which consisted
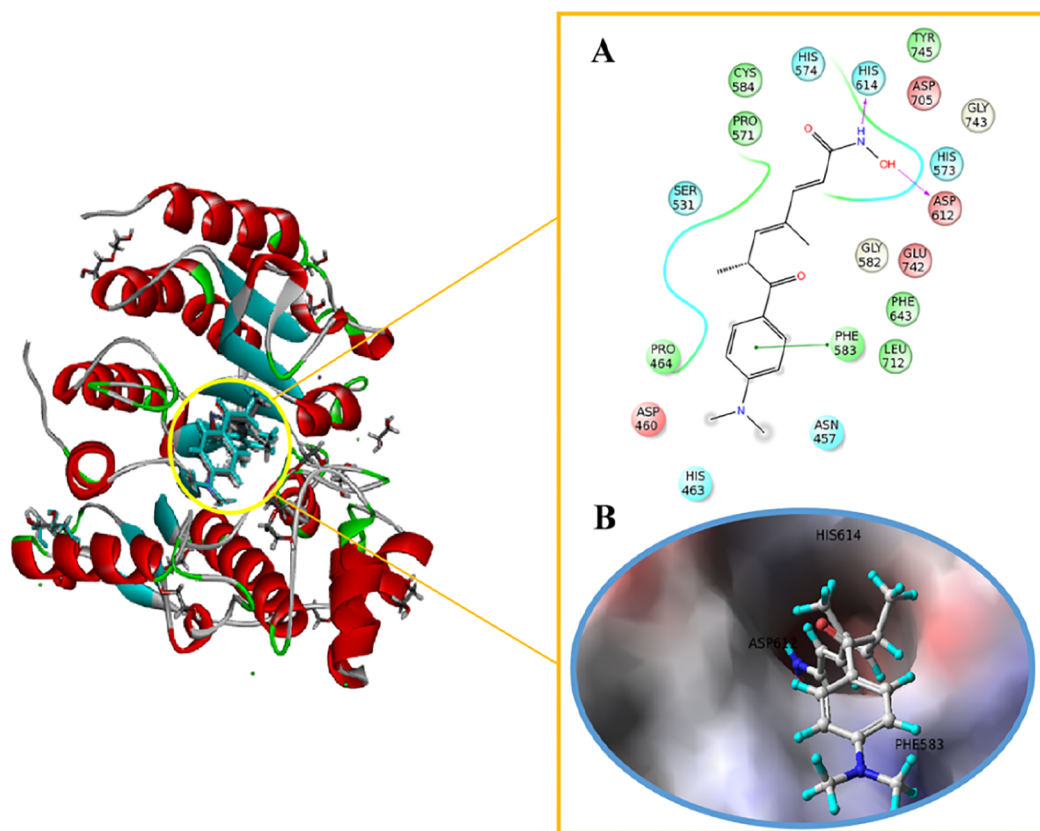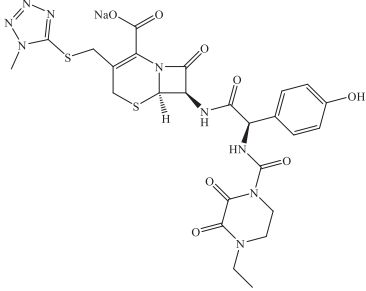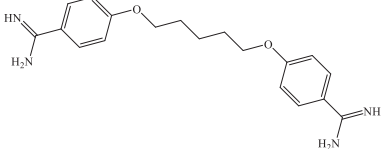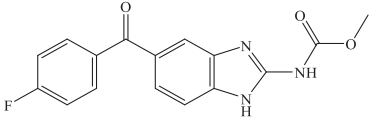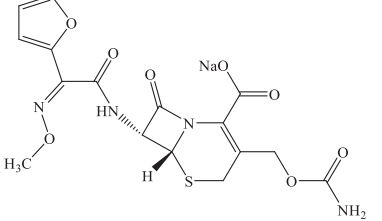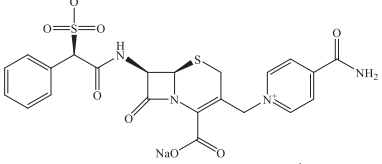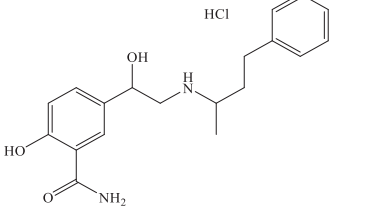

Fig. 3. Binding mode between the co-crystallized ligand and crystal structure of HDAC6 (PDB code: 5WGI). (A) 2D diagram illustrating the interactions. (B) Surface characteristic diagram illustrating the interactions.

Table 4
Inhibitory activities of screened compounds against HDAC6.

No.	CAS No.	Name	Structure	IC$_{50}$ (μM)[a]
1	62893-20-3	Cefoperazone Sodium		8.59 ± 1.06
2	100-33-4	Pentamidine		23.92 ± 0.98
3	31430-15-6	Flubendazole		1837 ± 2.63
4	56238-63-2	Cefuroxime Sodium		NA[b]
5	52152-93-9	Cefsulodin Sodium Salt		NA
6	32780-64-6	Labetalol Hydrochloride		NA

[a] Data are shown as the mean ± SD from three independent experiments.
[b] NA means no activity.

of two hydrogen bond acceptors and two hydrophobic groups, was the ideal pharmacophore hypothesis among the 10 pharmacophore hypotheses. Tubastatin A is a specific HDAC6 inhibitor with an IC$_{50}$ value of 15 nM, and A3 is the most active ligand in the decoy set with an IC$_{50}$ value of 1.76 nM. Fig. 2C and D revealed that all characteristics of pharmacophore hypothesis 7 was highly mapped with Tubastatin A and A3, indicating that the pharmacophore hypothesis 7 was reliable.

3.2. Virtual screening and molecular docking

The validated pharmacophore model was used to carry out the database screening from FDA Drugs Database. On the basis of pharmacophore model 7, 56 compounds with fit value > 3.00 were screened by ligand-based virtual screening (Table 2).

In order to avoid the false positive and improve the hit rate of

searching effective HDAC6 inhibitors, the 56 compounds were submitted for further molecular docking screening. Before conducting molecular docking screening, the original co-crystallized ligand was extracted and docked with the ligand binding region of the crystal structure (PDB code: 5WGI) to verify the reliability of this method. The RMSD between the co-crystallized ligand and the docked conformation of 5WGI was calculated as 1.87 Å. Furthermore, the hydroxylamine on the co-crystallized ligand acted as a hydrogen bond donor to emerge hydrogen bonds with the amino acid residues Asp612 and His614 (Fig. 3A). The aromatic ring on the co-crystallized ligand formed hydrophobic interaction with the hydrophobic amino acid residue Phe583. Fig. 3B displayed the surface characteristic of the binding mode between the co-crystallized ligand and the active site of crystal structure. This docking procedure had a high reliability in reproducing the co-crystal bioactive conformation of the HDAC6 inhibitor.
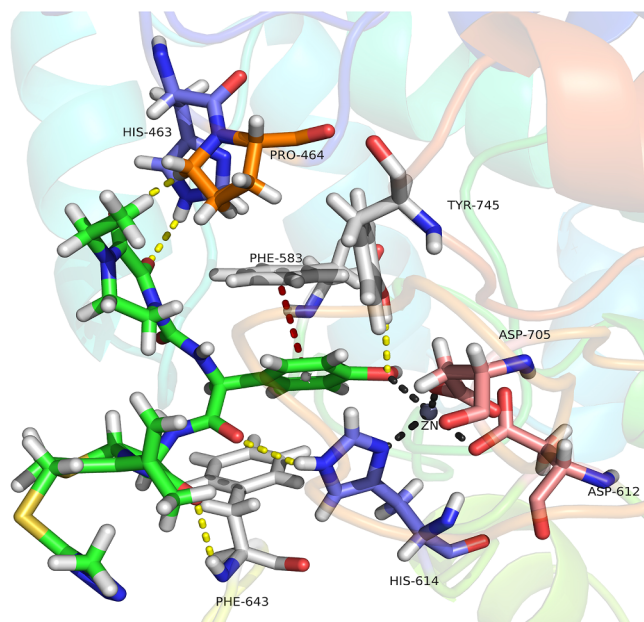
Fig. 4. Binding mode between cefoperazone sodium and the crystal structure of HDAC6 (PDB code: 5WGI). The crystal structure of HDAC6 is displayed in ribbons, and the compound is represented as stick. Zinc ion is represented by a gray ball. Metal coordination and hydrogen bond interactions are indicated by black and yellow dashed lines, respectively. (For interpretation of the references to colour in this figure legend, the reader is referred to the web version of this article.)
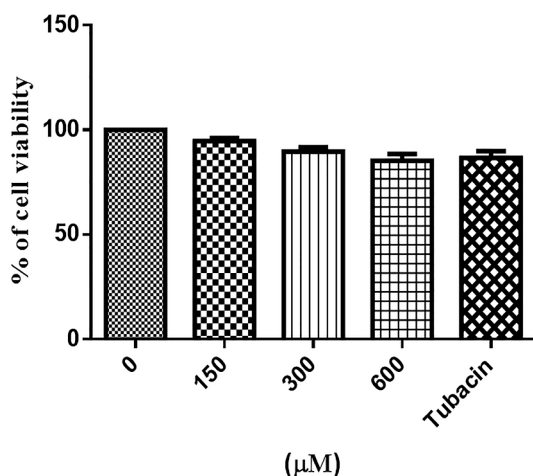

Fig. 5. Effects of cefoperazone sodium on proliferation of PANC-1 cells. Cell viability of PANC-1 cells after treatment with cefoperazone sodium or Tubacin (5 μM). Data are presented as mean ± SD, n = 3.

Therefore, 56 compounds were docked into the active sites of the receptor, and finally the 6 hit compounds (Table 3) with docking score > 7.00 were screened out. Pan assay interference compounds (PAINS) are defined as compounds that interfere with most tests. In order to exclude interference compounds, 6 screened compounds were assessed using the SwissADME online tool. The data (Fig. S3) showed that the PAINS of 6 compounds were all 0 alert. The top 6 hits in molecular docking were selected to further detect their inhibitory activity against HDAC6.

3.3. HDAC6 inhibitory effect evaluation

To further investigate the previous results, the inhibitory effects of 6 compounds on HDAC6 were preliminarily evaluated. The chemical

structures and biological activities of the hit compounds were listed in Table 4. According to the experimental results, cefoperazone sodium had a most strong binding inhibitory activity against HDAC6 as demonstrated by a 8.59 ± 1.06 μM of IC_{50} value. Similarly, cefoperazone sodium had the highest docking score in molecular docking. The experimental data were in good agreement with the docking results, further indicating that the screening results were reliable.

Molecular docking of cefoperazone sodium with other HDAC isoforms were performed subsequently. Up to now, 11 zinc-dependent HDAC isoforms have been discovered, and the crystal structures of 9 HDAC isoforms including HDAC1, 2, 3, 4, 5, 6, 7, 8 and 10 were reported in the Protein Data Bank. Except for HDAC3 and HDAC5, the binding sites of small molecule inhibitors were found in the crystal structures of all other HDAC isoforms. Therefore, HDAC1, 2, 4, 6, 7, 8 and 10 were selected for molecular docking studies. On the one hand, the results (Table S3) indicated that the docking scores of cefoperazone sodium with HDAC1, HDAC6 and HDAC8 were relatively higher. On the other hand, the docking scores of cefoperazone sodium with HDAC1 and HDAC8 were obviously lower than that of their co-crystallized ligands, while the docking effect of cefoperazone sodium with HDAC6 was the best. Accordingly, it was speculated that cefoperazone sodium presented higher selectivity for HDAC6.

Cefoperazone sodium, the third-generation cephalosporin, has a good antibacterial effect, but its inhibitory activity on HDAC6 has not been reported. Therefore, it was of great significance to analyze the binding mode (Fig. 4) of cefoperazone sodium with the crystal structure (PDB code: 5WGI) in detail. The aromatic ring on cefoperazone sodium formed π-π interaction with the hydrophobic amino acid residue Phe583. In the HDAC6 active site, cefoperazone sodium could form hydrogen bonds with the amino acid residues His614, Phe643, Pro464, Tyr745 and His463. The screened compound, cefoperazone sodium, has different chemical scaffold with the co-crystallized ligand, but it exhibits similar binding pattern at the active site, including Phe583, Asp612 and His614. The zinc-binding mode of cefoperazone sodium with HDAC6 was showed in Fig. 4. The hydroxyl group of cefoperazone sodium and the amino acid residues Asp612, Asp705 and His614 of HDAC6 could form coordination with zinc ion in the active site. The result reveals that these key amino acid residues may be critical for inhibiting the activity of HDAC6. This discovery may have important implications for the structural design and modification of novel HDAC6 inhibitors in the future.

3.4. Anti-metastatic experiments of cefoperazone sodium

It is reported that HDAC6 plays a crucial role in invasion and metastasis of cancer, and the high expression of HDAC6 is associated with accelerated metastasis and increased invasiveness of cancer cells [31]. Accordingly, the effect of cefoperazone sodium on the migration and invasion of human pancreatic cancer PANC-1 cells were further investigated.

3.4.1. Cefoperazone sodium had no effect on the proliferation of PANC-1 cells

In order to exclude the effect of cefoperazone sodium on cell proliferation, MTT assay was used to detect the non-cytotoxic concentration of cefoperazone sodium for subsequent cell migration and invasion experiments. PANC-1 cells were incubated with 150, 300 and 600 μM of cefoperazone sodium for 48 h, and then MTT assay was performed to detect the cell viability. The results (Fig. 5) displayed that 150–600 μM of cefoperazone sodium had no cytotoxicity effect on PANC-1 cells. 5 μM of tubacin, a specific HDAC6 inhibitor, showed no cytotoxicity on PANC-1 cells as a positive control. Therefore, the concentrations of cefoperazone sodium lower than 600 μM were selected for subsequent experiments.
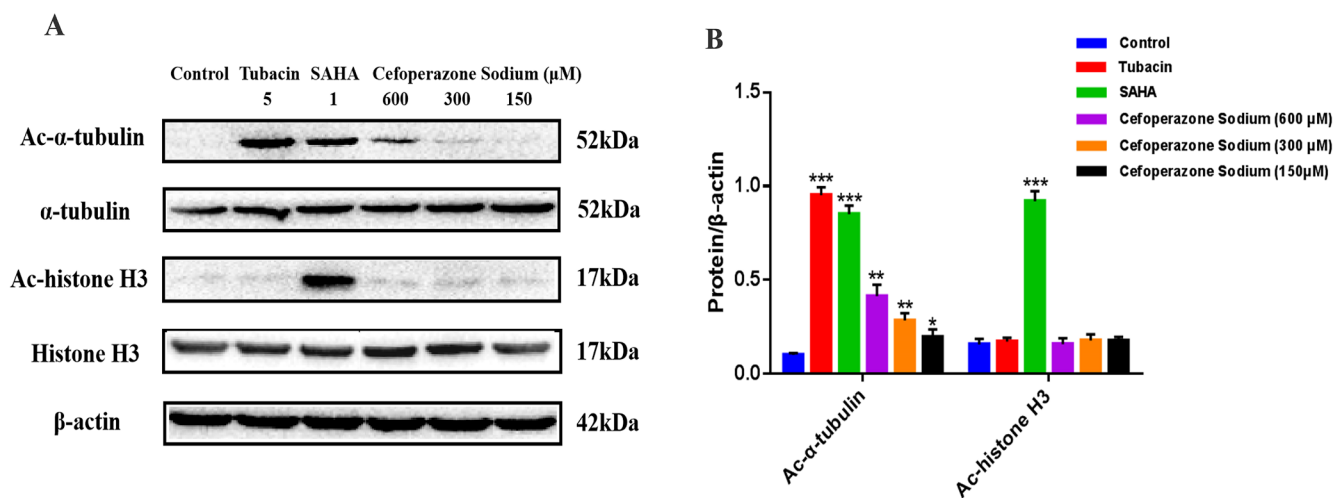
A

B

Fig. 6. Immunoblotting analysis of PANC-1 cells extracts after treated with Tubacin, SAHA and cefoperazone sodium for 48 h. Data are shown as the mean ± SD from three independent experiments. * $p < 0.05$, ** $p < 0.01$, *** $p < 0.001$ vs. control group.
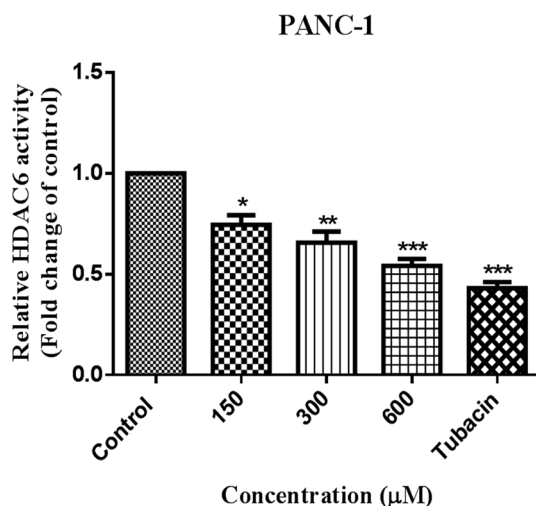

Fig. 7. The impact of cefoperazone sodium and Tubacin (5 μM) on HDAC6 activity in PANC-1 cells. Data are shown as the mean ± SD from three independent experiments. * $p < 0.05$, ** $p < 0.01$, *** $p < 0.001$ vs. control group.

3.4.2. Cefoperazone sodium selectively inhibited HDAC6 in the cellular environment

It has been reported that pan-HDAC inhibitors can induce the hyperacetylation of histone and non-histone proteins, such as the hyperacetylation of histone H3 and α-tubulin. However, the deacetylase activity of HDAC6 is mainly focused on non-histone substrates, and selective HDAC6 inhibitors can significantly catalyze the hyperacetylation of α-tubulin, but not histone H3.

To demonstrate the selective inhibitory effect of cefoperazone sodium on HDAC6, we investigated the effects of cefoperazone sodium on acetylated-α-tubulin and acetylated-histone H3 in PANC-1 cells. The experimental results (Fig. 6) showed that cefoperazone sodium, pan-HDAC inhibitor SAHA and HDAC6 specific inhibitor tubacin induced an increase of acetylated-α-tubulin, but only the pan-HDAC inhibitor SAHA could produce a massive increase in acetylated-histone H3. In addition, cefoperazone sodium induced dose-dependent increase of acetylated-α-tubulin. These data indicated that cefoperazone sodium could selectively inhibit HDAC6 in the cellular environment.

3.4.3. Cefoperazone sodium inhibited HDAC6 activity in PANC-1 cells

PANC-1 cells were treated with different concentrations of cefoperazone sodium (at 150, 300 and 600 μM) and Tubacin (at 5 μM) for 48 h. The experimental data (Fig. 7) showed that cefoperazone sodium inhibited HDAC6 activity in PANC-1 cells in a dose-dependent manner.

3.4.4. Cefoperazone sodium inhibited the migration and invasion of PANC-1 cells

To investigate the effect of cefoperazone sodium on the cell migration and invasion of human pancreatic cancer cells, wound healing and transwell chamber experiments were subsequently performed. PANC-1 cells were incubated with different concentrations of cefoperazone sodium (at 150, 300 and 600 μM) or tubacin at 5 μM for 48 h. Wound healing assays were used to detect the inhibition of the compounds on cell migration. Cefoperazone sodium could significantly inhibit pancreatic cancer cells migration into the wound as shown in Fig. 8A. The results revealed that cefoperazone sodium inhibited the migration ability of PANC-1 cells in a dose-dependent manner. The transwell chamber assays indicated that the average number of PANC-1 cells invading through the membrane treated with cefoperazone sodium were obviously decreased compared to the control group (Fig. 8B). Consistent with the results of wound healing experiments, cefoperazone sodium inhibited the invasion ability of PANC-1 cells in a dose-dependent manner. In conclusion, the above results indicated that cefoperazone sodium can evidently inhibit the migration and invasion of PANC-1 cells.

4. Conclusion

HDAC6 is reported to play a significant role in the invasion and metastasis of cancer, and is necessary for carcinogenic transformation and cancer formation. The high expression of HDAC6 is associated with accelerated metastasis and increased invasiveness of cancer cells, and HDAC6 inhibitors can be used in cancer therapy by inhibiting the activity of HDAC6. Up to present, the HDAC6 inhibitors that have been reported are extremely limited, so specific HDAC6 inhibitors need to be discovered urgently.

In our research, virtual screening combined with pharmacophore model was used to identify selective HDAC6 inhibitors from FDA Drugs Database. The screened compounds were docked with the crystal structure of HDAC6 via molecular docking to improve the hit rate in the databases screening based on pharmacophore model. Subsequently, the HDAC6 inhibitory activity of the hit compounds were preliminarily evaluated using the enzymatic assay, and finally cefoperazone sodium was selected for further experiments. Cefoperazone sodium was docked
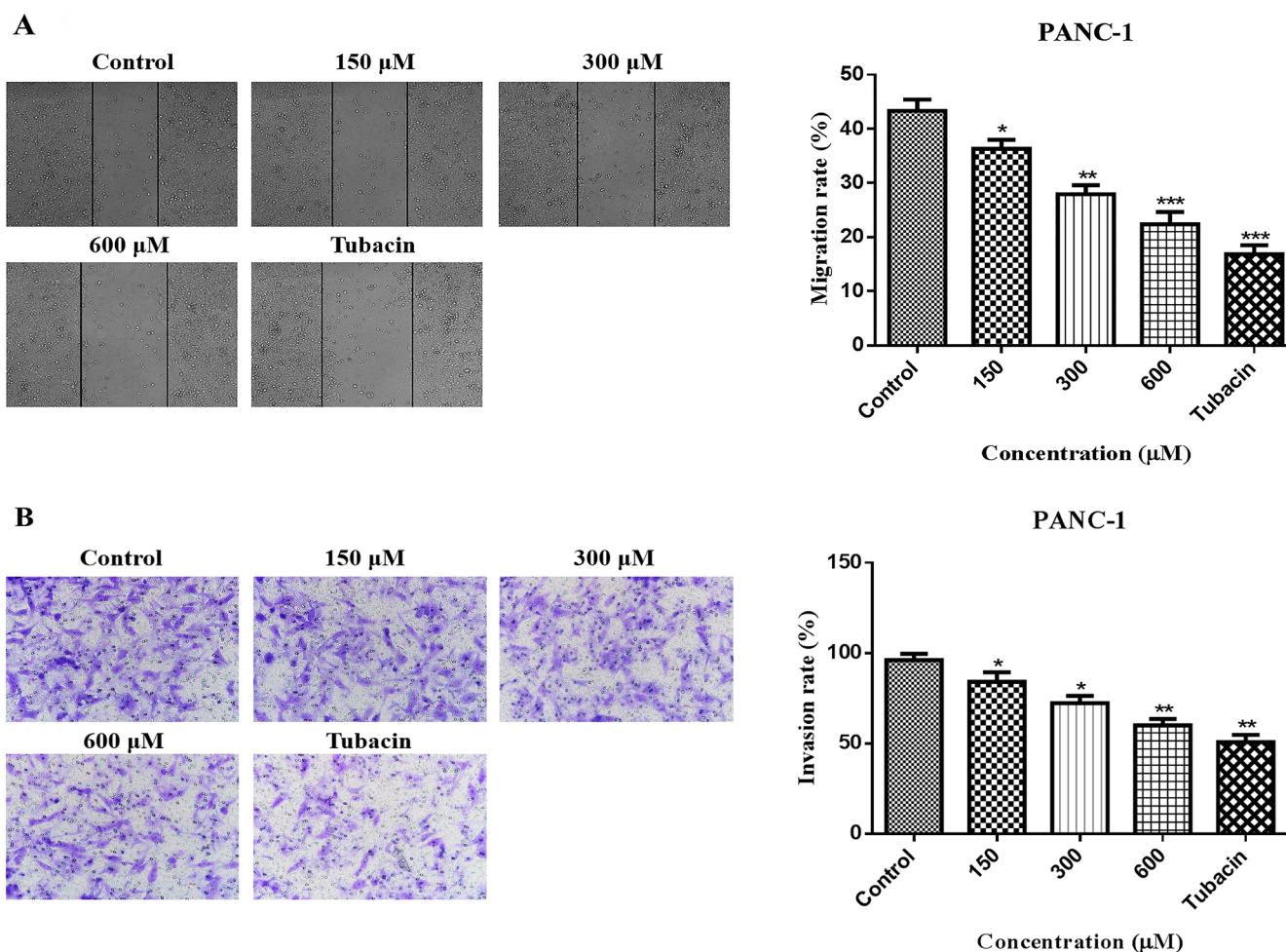
Fig. 8. Cefoperazone sodium inhibited the migration and invasion of PANC-1 cells. (A) Wound healing assays were used to investigate the effect of cefoperazone sodium and Tubacin (5 μM) on the migration of PANC-1 cells. (B) Transwell chamber assays were used to investigate the effect of cefoperazone sodium and Tubacin (5 μM) on the invasion of PANC-1 cells. Data are shown as the mean ± SD from three independent experiments. $* p < 0.05$, $** p < 0.01$, $*** p < 0.001$ vs. control group.

with the crystal structures of HDAC isoforms via molecular docking to investigate its selectivity to HDAC6, and we found that the docking effect of cefoperazone sodium with HDAC6 was the best. Furthermore, immunoblotting analysis showed that cefoperazone sodium could selectively inhibit HDAC6 in the cellular environment, indicating that cefoperazone sodium was a specific inhibitor of HDAC6. The non-cytotoxic concentration of cefoperazone sodium was used to investigate the inhibitory effect of HDAC6 activity and the effect on the migration and invasion of pancreatic cancer cells. The experimental results illustrated that cefoperazone sodium can evidently inhibit the migration and invasion of PANC-1 cells. High expression of HDAC6 is associated with accelerated metastasis and increased invasiveness of cancer cells. Therefore, it can be speculated that cefoperazone sodium inhibited the migration and invasion of PANC-1 cells by inhibiting the activity of HDAC6 in PANC-1 cells.

This study provides a systematic virtual screening method and the reliability of docking results were verified by HDAC6 inhibitory activity assay. The binding patterns of inhibitors at the active site of the crystal structure was revealed by molecular docking, providing a reference value for the structural design and optimization of HDAC6 inhibitors. This research not only discovered the new therapeutic effect of cefoperazone sodium in targeted inhibition of HDAC6 activity, but also provided a practical strategy for searching effective HDAC6 inhibitors for the treatment of cancer.

Declaration of Competing Interest

The authors declare that they have no known competing financial interests or personal relationships that could have appeared to influence the work reported in this paper.

Acknowledgement

Appendix A. Supplementary material

Supplementary data to this article can be found online at https://doi.org/10.1016/j.bioorg.2020.103679.

References

[1] X.J. Yang, E. Seto, The Rpd3/Hda1 family of lysine deacetylases: from bacteria and yeast to mice and men, Nat. Rev. Mol. Cell Biol. 9 (2008) 206–218.
[2] C. Scholz, B.T. Weinert, S.A. Wagner, P. Beli, Y. Miyake, J. Qi, et al., Acetylation site specificities of lysine deacetylase inhibitors in human cells, Nat. Biotechnol. 33

(2015) 415–423.

[3] B.E. Gryder, Q.H. Sodji, A.K. Oyelere, Targeted cancer therapy: giving histone deacetylase inhibitors all they need to succeed, Future Med. Chem. 4 (2012) 505–524.

[4] C. Felice, A. Lewis, A. Armuzzi, J.O. Lindsay, A. Silver, Review article: selective histone deacetylase isoforms as potential therapeutic targets in inflammatory bowel diseases, Aliment. Pharmacol. Ther. 41 (2015) 26–38.

[5] C.H. Arrowsmith, C. Bountra, P.V. Fish, K. Lee, M. Schapira, Epigenetic protein families: a new frontier for drug discovery, Nat. Rev. Drug Discovery 11 (2012) 384–400.

[6] X. Zhang, Z. Yuan, Y. Zhang, S. Yong, A. Salas-Burgos, J. Koomen, et al., HDAC6 modulates cell motility by altering the acetylation level of cortactin, Mol. Cell 27 (2007) 197–213.

[7] A. Matsuyama, T. Shimazu, Y. Sumida, A. Saito, Y. Yoshimatsu, D. Seigneurin-Berny, et al., In vivo destabilization of dynamic microtubules by HDAC6-mediated deacetylation, EMBO J. 21 (2002) 6820–6831.

[8] L. Santo, T. Hideshima, A.L. Kung, J.C. Tseng, D. Tamang, M. Yang, et al., Preclinical activity, pharmacodynamic, and pharmacokinetic properties of a selective HDAC6 inhibitor, ACY-1215, in combination with bortezomib in multiple myeloma, Blood 119 (2012) 2579–2589.

[9] H.Y. Lee, J.F. Lee, S. Kumar, Y.W. Wu, W.C. HuangFu, M.J. Lai, et al., 3-Aroylindoles display antitumor activity in vitro and in vivo: Effects of N1-substituents on biological activity, Eur. J. Med. Chem. 125 (2017) 1268–1278.

[10] K.V. Butler, J. Kalin, C. Brochier, G. Vistoli, B. Langley, A.P. Kozikowski, Rational design and simple chemistry yield a superior, neuroprotective HDAC6 inhibitor, tubastatin A, J. Am. Chem. Soc. 132 (2010) 10842–10846.

[11] N.J. Porter, A. Mahendran, R. Breslow, D.W. Christianson, Unusual zinc-binding mode of HDAC6-selective hydroxamate inhibitors, PNAS 114 (2017) 13459–13464.

[12] C.M. Song, S.J. Lim, J.C. Tong, Recent advances in computer-aided drug design, Briefings Bioinf. 10 (2009) 579–591.

[13] R.A. Friesner, R.B. Murphy, M.P. Repasky, L.L. Frye, J.R. Greenwood, T.A. Halgren, et al., Extra precision glide: docking and scoring incorporating a model of hydrophobic enclosure for protein-ligand complexes, J. Med. Chem. 49 (2006) 6177–6196.

[14] M.K.W. Mackwitz, A. Hamacher, J.D. Osko, J. Held, A. Scholer, D.W. Christianson, et al., Multicomponent Synthesis and Binding Mode of Imidazo[1,2-a]pyridine-Capped Selective HDAC6 Inhibitors, Org. Lett. 20 (2018) 3255–3258.

[15] J.H. Lee, Y. Yao, A. Mahendran, L. Ngo, G. Venta-Perez, M.L. Choy, et al., Creation of a histone deacetylase 6 inhibitor and its biological effects [corrected], Proc. Nat. Acad. Sci. USA 112 (2015) 12005–12010.

[16] M. Faria Freitas, M. Cuendet, P. Bertrand, HDAC inhibitors: a 2013-2017 patent survey, Expert Opin. Therapeutic Patents (2018) 1–17.

[17] C.A. Simoes-Pires, P. Bertrand, M. Cuendet, Novel histone deacetylase 6 (HDAC6) selective inhibitors: a patent evaluation (WO2014181137), Expert Opin. Ther. Pat. 27 (2017) 229–236.

[18] A.I. Uba, K. Yelekci, Carboxylic acid derivatives display potential selectivity for human histone deacetylase 6: Structure-based virtual screening, molecular docking and dynamics simulation studies, Comput. Biol. Chem. 75 (2018) 131–142.

[19] M. Leonhardt, A. Sellmer, O.H. Kramer, S. Dove, S. Elz, B. Kraus, et al., Design and biological evaluation of tetrahydro-beta-carboline derivatives as highly potent histone deacetylase 6 (HDAC6) inhibitors, Eur. J. Med. Chem. 152 (2018) 329–357.

[20] O. Rabal, J.A. Sanchez-Arias, M. Cuadrado-Tejedor, I. de Miguel, M. Perez-Gonzalez, C. Garcia-Barroso, et al., Design, synthesis, biological evaluation and in vivo testing of dual phosphodiesterase 5 (PDE5) and histone deacetylase 6 (HDAC6)-selective inhibitors for the treatment of Alzheimer's disease, Eur. J. Med. Chem. 150 (2018) 506–524.

[21] J. Yang, G. Cheng, Q. Xu, S. Luan, S. Wang, D. Liu, et al., Design, synthesis and biological evaluation of novel hydroxamic acid based histone deacetylase 6 selective inhibitors bearing phenylpyrazol scaffold as surface recognition motif, Bioorg. Med. Chem. 26 (2018) 1418–1425.

[22] Y. Miyake, J.J. Keusch, L. Wang, M. Saito, D. Hess, X. Wang, et al., Structural insights into HDAC6 tubulin deacetylation and its selective inhibition, Nat. Chem. Biol. 12 (2016) 748–754.

[23] D. Shivakumar, J. Williams, Y. Wu, W. Damm, J. Shelley, W. Sherman, Prediction of absolute solvation free energies using molecular dynamics free energy perturbation and the OPLS force field, J. Chem. Theory Comput. 6 (2010) 1509–1519.

[24] S. Sakkiah, S. Thangapandian, S. John, Y.J. Kwon, K.W. Lee, 3D QSAR pharmacophore based virtual screening and molecular docking for identification of potential HSP90 inhibitors, Eur. J. Med. Chem. 45 (2010) 2132–2140.

[25] H.Z. Xie, L.Y. Liu, J.X. Ren, J.P. Zhou, R.L. Zheng, L.L. Li, et al., Pharmacophore modeling and hybrid virtual screening for the discovery of novel IkappaB kinase 2 (IKK2) inhibitors, J. Biomol. Struct. Dyn. 29 (2011) 165–179.

[26] G.M. Sastry, M. Adzhigirey, T. Day, R. Annabhimoju, W. Sherman, Protein and ligand preparation: parameters, protocols, and influence on virtual screening enrichments, J. Comput. Aided Mol. Des. 27 (2013) 221–234.

[27] M. Wang, W. Li, Y. Wang, Y. Song, J. Wang, M. Cheng, In silico insight into voltage-gated sodium channel 1.7 inhibition for anti-pain drug discovery, J. Mol. Graph. Model. 84 (2018) 18–28.

[28] B. Heltweg, F. Dequiedt, B.L. Marshall, C. Brauch, M. Yoshida, N. Nishino, et al., Subtype selective substrates for histone deacetylases, J. Med. Chem. 47 (2004) 5235–5243.

[29] T. Suzuki, A. Kouketsu, Y. Itoh, S. Hisakawa, S. Maeda, M. Yoshida, et al., Highly potent and selective histone deacetylase 6 inhibitors designed based on a small-molecular substrate, J. Med. Chem. 49 (2006) 4809–4812.

[30] D.V. Smil, S. Manku, Y.A. Chantigny, S. Leit, A. Wahhab, T.P. Yan, et al., Novel HDAC6 isoform selective chiral small molecule histone deacetylase inhibitors, Bioorg. Med. Chem. Lett. 19 (2009) 688–692.

[31] Y.S. Lee, K.H. Lim, X. Guo, Y. Kawaguchi, Y. Gao, T. Barrientos, et al., The cytoplasmic deacetylase HDAC6 is required for efficient oncogenic tumorigenesis, Cancer Res. 68 (2008) 7561–7569.